# Monolithic integration of quantum cascade laser, quantum cascade detector, and subwavelength waveguides for mid-infrared integrated gas sensing

Swapnajit Chakravarty\*, a, Jason Midkiff<sup>b</sup>, Kyoungmin Yoo<sup>b</sup>, Ali Rostamian<sup>b</sup>, Ray T. Chen \*, a,b a Omega Optics Inc., 8500 Shoal Creek Blvd., Bldg. 4, Suite 200,, Austin, TX, USA 78757 b Dept. of Electrical and Computer Engineering, University of Texas, 10100 Burnet Road Bldg. 160, Austin, TX, USA 78758;

#### **ABSTRACT**

Mid-infrared trace gas sensing is a rapidly developing field with wide range of applications. Although CRDS, TDLAS, FTIR and others, can provide parts per billion and in some cases, parts per trillion sensitivities, these systems require bulky and expensive optical elements and, furthermore, are very sensitive to beam alignment and have significant size and weight that place constrains on their applications in the field, particularly for airborne or handheld platforms. Monolithic integration of light sources and detectors with an optically transparent passive photonics platform is required to enable a compact trace gas sensing system that is robust to vibrations and physical stress. Since the most efficient quantum cascade lasers (QCLs) demonstrated are in the InP platform, the choice of InGaAs-InP for passive photonics eliminates the need for costly wafer bonding versus silicon, germanium of GaAs, that would require optically absorbing bonding interfaces. The InGaAs-InP material platform can potentially cover the entire λ=3-15μm molecular fingerprint region. In this paper, we experimentally demonstrate monolithic integration of QCL, quantum cascade detector (QCD) and suspended membrane sub-wavelength waveguides in a fully monolithic InGaAs/InP material system. The transverse magnetic polarized QCL emission is efficiently coupled into an underlying InGaAs suspended membrane subwavelength waveguide. In addition to low-loss compact waveguide bends, the suspended membrane architecture offers a high analyte overlap integral with the analyte. The propagating light is absorbed at the peak absorbance wavelength of the selected analyte gas and the transduced signal is detected by the integrated QCD. Gas sensing will be demonstrated.

**Keywords:** spectroscopy, subwavelength waveguide, quantum cascade laser, quantum cascade detector, sensing, monolithic integration.

\*swapnajit.chakravarty@omegaoptics.com, <a href="mailto:chenrt@austin.utexas.edu">chenrt@austin.utexas.edu</a>; phone 1 512 996 8833; fax 1 512-471-8575;

#### 1. INTRODUCTION

Mid-infrared trace gas sensing is a rapidly developing field with wide range of applications. Although cavity ring-down spectroscopy (CRDS) [1], tunable diode laser absorption spectroscopy (TDLAS) [2], Fourier transform infrared spectroscopy (FTIR) [3] and others, can provide parts per billion (ppb) and in some cases, parts per trillion (ppt) sensitivities, these systems require bulky and expensive optical elements and, furthermore, are very sensitive to beam alignment and have significant size and weight that place constrains on their applications in the field, particularly for airborne or handheld platforms. Monolithic integration of light sources and detectors with an optically transparent passive photonics platform is required to enable a compact trace gas sensing system that is robust to vibrations and physical stress. Since the most efficient quantum cascade lasers (QCLs) demonstrated are in the InP platform, the choice of InGaAs-InP for passive photonics eliminates the need for costly wafer bonding to silicon, germanium of GaAs. More importantly, the wafer bonding processes, that have demonstrated feasibility till date use silicon dioxide or polymers as the adhesive bonding interface that have high optical absorbance for much of the mid-IR. Silicon dioxide absorbs for  $\lambda$ >3.7 $\mu$ m. Most polymers are characterized by high absorbance for  $\lambda$ >5 $\mu$ m. The InGaAs-InP material platform can potentially cover the entire  $\lambda$ =3-15 $\mu$ m molecular fingerprint region.

We developed the physics of on-chip absorption spectroscopy using slow light enhanced slotted photonic crystal waveguides to enhance the interaction between light and analyte [4, 5]. According to the Beer-Lambert-Bouguer technique, transmitted intensity I is given by

$$I = I_0 \exp(-\gamma \alpha L) \tag{1}$$

where I0 is the incident intensity,  $\alpha$  is the absorption coefficient of the medium, L is the interaction length and  $\gamma$  is the medium-specific absorption factor determined by dispersion enhanced light-matter interaction. In conventional systems, L must be large to achieve a suitable sensitivity of the measured I/I<sub>0</sub>. For lab-on-chip systems, L must be small, hence  $\gamma$  must be large. Using perturbation theory, it was shown [6]:

$$\gamma = f \times \frac{c/n}{v_g} \tag{2}$$

where c is the velocity of light in free space, vg is the group velocity in the medium of effective index n and f is the filling factor denoting the relative fraction of the optical field residing in the analyte medium.

We experimentally demonstrated that slotted photonic crystal waveguides (PCWs) can enable high sensitivity gas sensing on chip via absorption spectroscopy. We detected 3 parts per million (ppm) greenhouse gas carbon monoxide (CO) at  $\lambda$ =4.55 $\mu$ m with feasibility to detect down to sub-100 parts per billion (ppb) by nominal device modifications in a silicon-on-sapphire (SoS) platform [7]. We also detected the chemical warfare simulant triethylphosphate (TEP) down to 10ppm at  $\lambda$ =3.4µm also in a SoS platform [8]. Recently, we experimentally demonstrated the detection of ammonia at  $\lambda$ =6.15 um in an InGaAs-InP platform and alcohol at  $\lambda$ =3.4 um in a SOI platform, using enhanced analyte overlap integrals in nanophotonic structures. The emission from a QCL is transverse magnetic (TM) polarized which necessitates a polarization rotator to be simultaneously included on chip to enable integration with the transverse electric (TE) guiding holes-in-a-slab configuration dielectric photonic crystals. Sub-wavelength waveguides (SWWs) present a class of low-loss corrugated waveguides with sub-wavelength corrugation periodicity that also enables large analyte overlap integrals in their holey architecture. Although SWWs do not provide a slow light effect as in PCWs, our preliminary results indicate that SWWs ~3-4 times longer than a corresponding PCW can potentially compensate for the lack of group velocity reduction and achieve similar gas sensing sensitivities using optical absorbance. The use of SWWs eliminates insertion losses typical in a well-compensated PCW structure due to group velocity mismatch between regular strip waveguides and PCWs. Furthermore, in contrast to PCWs where any bend in the waveguide introduces significant loss, compact 90-degree bends with <30um bend radius in SWWs allows an efficient utilization of chip epi. The alldielectric waveguide sensing also eliminates high propagation losses inherent in integrated systems using plasmonic waveguides [9].

In this paper, we experimentally demonstrate monolithic integration of QCL, quantum cascade detector (QCD) and suspended membrane sub-wavelength waveguides in a fully monolithic InGaAs/InP material system. Our initial work in monolithic integration (determined by epi availability) is at  $\lambda$ =4.6 $\mu$ m centered on the CO absorbance maxima. The transverse magnetic polarized QCL emission is efficiently coupled into an underlying InGaAs suspended membrane subwavelength waveguide. In addition to low-loss compact waveguide bends, the suspended membrane architecture offers a high analyte overlap integral with the analyte.

# 2. COMPARISON OF EXISTING TECHNIQUES

Fig. 1 shows a schematic of the handheld/ portable device  $(7''\times4''\times3'')$  currently in development as a generalized platform to cover all wavelengths in the  $\lambda$ =3-15 $\mu$ m fingerprint region. Customized electronics can further reduce dimensions that will allow easy integration with Group 1 fixed wing and quadcopter SUAS  $(2''\times2''\times1'')$ . The generalized epi comprises a passive undoped InGaAs waveguiding section (center) and the active QCL (left) and QCD sections (right). Light is coupled in between active and passive regions via adiabatically tapered waveguide couplers.

The size, weight and power (SWaP) benefits of SPCW system over table-top multi-pass cell systems are illustrated in Tables 1 and Table 2. Spectral signatures of most gases in our environment, either naturally or through chemical reactions, have been studied widely for many decades. Absorption spectroscopy [10], X-Ray spectroscopy [11], Raman spectroscopy [12] techniques are highly accurate, but require bulky apparatus and complex optical alignments that limit their ability for portable monitoring. A primary requirement in such methods is a gas cell which is > 3 feet long thereby making them large, heavy, ungainly and not portable.

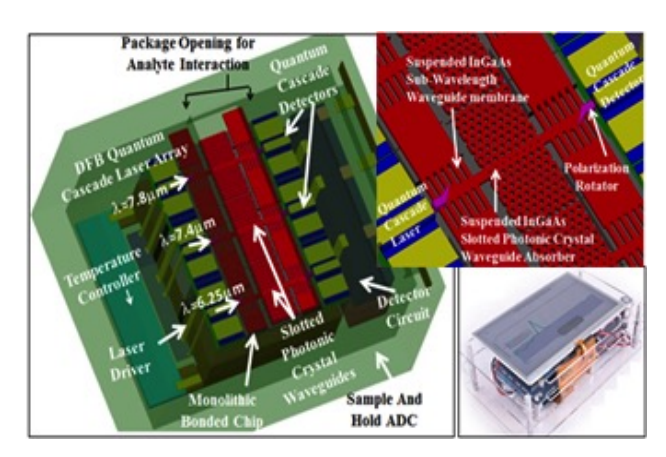


Figure 1: Schematic of the packaged analyzer unit, integrated with data display. (top right) magnified schematic of the analyzer showing monolithically packaged quantum cascade laser (QCL) array, quantum cascade detector (QCD) array, and suspended membrane slow light enhanced slotted photonic crystal gas waveguide (SPCW) absorbers. Electronics are integrated into a compact package. A unit demonstrated at University of Texas, Austin is shown in (bottom right) with integrated electronics to drive the laser/detector/transducer system, as well as to control display and enable Bluetooth data porting.

Some sensing techniques do not use gas cells; optical fiber based evanescent sensing [13] and photonic crystal fiber based refractive index sensing [14], are good for remote monitoring, however weak evanescent interaction [29] and difficulty in filing photonic crystal fibers with gases [14] limits their practical implementation. In recent years, QCLs are operating in the mid-IR, where most molecules have strong fundamental absorption signatures [15]. However, a gas cell is still necessary for absorption of light, which still keeps system volume large (~0.5 meters) [15] and unwieldy. Openpath configurations using QCLs have also been studied which however need precisely positioned retro-reflectors and line-of-sight operation [16], both conditions that are unrealistic for trace chemical nerve agent detection in a random threat. In Table 1, we show the versatility of our proposed research.

Table 1: Comparison of existing sensing and spectral analysis techniques

	<u> </u>		1	
Features <sup>†</sup>	Bulk spectroscopy*	Quantum Cascade Laser	Optical Fiber Sensing	Proposed Approach
Gas Cell Requirement	Yes (-)	Yes (-)	No (+)	No (+)
Bulk Optics/ High Reflectivity Mirrors/ Specialized Windows	Yes (-)	Yes (-)	No (+)	No (+)
Line of Sight Measurement	Yes (-)	Yes (-)	No (+)	No (+)
Identification based on Spectral Signature	Yes (+)	Yes (+)	No (-)	Yes (+)
Spectroscopy System on Chip (portable)	No (-)	No (-)	No (-)	Yes (+)
Sensitivity	High (+)	High (+)	Medium (-)	High (+)

<sup>\*</sup>Bulk spectroscopy includes X-Ray scattering, Raman scattering, and all absorption methods that employ gas cells and bulky optical elements such as mirrors and lenses for signal transmission and detection.

Table 2: Comparison of proposed device with other optical spectroscopy techniques

Property	CRDS [1]	TDLAS [2]	FTIR [3]	PAS [17]	SPCW
On-Chip	No	No	No	No	Yes
Size	~1 cu. ft.	~0.5 cu. ft.	~1.4 cu. ft.	~1 cu. ft.	~24 cu. inches
Weight	~28lbs	~6lbs	~24lbs	~33lbs	< 21bs
Power (single gas)	200 Watt	0.5 Watt	40 Watt	90 Watt	~10Watt
Detection Limit (CH <sub>4</sub> )	(Halo) 4ppb	1ppm-m	15ppb	27ppb	2ppb
Portability	No	No*	No	No	Yes

<sup>&</sup>lt;sup>1</sup>A negative attribute is denoted in **Red** (-) while a positive attribute is denoted in **Green** (+).

Table 2 shows that our proposed research provides the best solution for miniaturized monolithic integration and spectroscopy with high sensitivity. Our proposed research combines the light-weight, small volume (~1.5cm ×0.5cm) chip with a laser and detectors for input and output coupling of light. Both features allow high density monolithic integration. In Table 2, we compare some of the features of common commercially available bulk absorption spectrometers. The technologies CRDS, TDLAS, FTIR and PAS are compared with our SPCW absorption spectroscopy device.

No technology exists, other than our proposed and demonstrated SPCW device, that enables not only the miniaturization as afforded by the slow light enhancement effects but also the enhanced optical mode overlap with the analyte on a chip-scale platform as afforded by our SPCW architecture. In addition, the chip-integrated enhanced optical interaction enables a monolithic device fabrication strategy that will significantly reduce the cost of high volume manufacturing. Table 2 shows that our SPCW spectrometer offers SWaP benefits unmatched by existing technologies. While enabling parts per trillion (ppt) sensitivities similar to CRDS, our platform can make use of the large absorption cross-sections in the mid-IR without requirements on mirror reflectivities and fragile optical alignment of free-space optics in other systems.

# 3. COMPARISON OF CHIP SIZE VERSUS MANUFACTURING COST

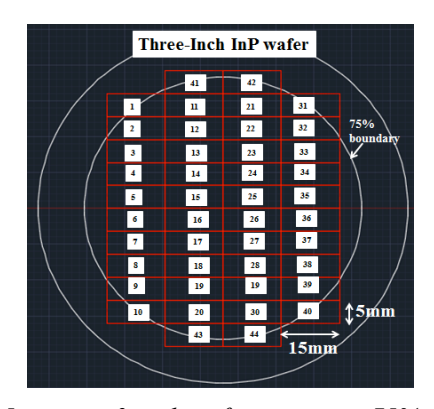


Fig. 2: Layout of dies 15mm×5mm on a 3-inch wafer, assuming 75% coverage of dies on the epi wafer. (44 useful dies)

Table 3: Cost comparison of complete monolithic, hybrid monolithic and non-monolithic devices integrating laser arrays, detector arrays and passive waveguide sensors

arrays, acceptor arrays and passive wavegarde sensors						
	Complete	Hybrid Monolithic (Integrated laser and	Non-Monolithic (separate laser			
	Monolithic	detector with bonded passive sensors)	and detector and gas cell) [18]			
Size of single die	15mm×5mm	4mm×5mm (or, 15mm×5mm†)	16mm×3mm (or,			
			16mm×30mm ††)			
Number of dies in 3-	(As Per Fig. 2)	~175 (or, 44 †)	~75 (or, ~8 ††)			
inch wafer	44					
Manufacturing cost	\$400	\$100 (or, \$400 †)	\$240 (or, \$2,250 ††)			
per die on III-V						
Additional Cost:	NA	\$400 per bond (Yield Questionable);	NA			
Wafer Bonding		(\$800 if bonding both QCL and detector				
		separately)**				
Alignment	NA	NA	Fragile alignments needed			
Requirement			between gas cell and laser and			
			detector, unsuitable for harsh			
			environment.			
Gas Sensitivity	Very High	Very High (PCW)	Poor (Strip Waveguide), Varies			
	(PCW)		with Wavelength			
Total Cost	\$400	\$900	\$450			
(Δλ~1μm)						

In Table 3, we compare the manufacturing cost of completely monolithic approach (in our proposed method) versus hybrid monolithic approach (such as bonding of III-V to group IV semiconductors). We also include a third column for hybrid approaches with separate quantum cascade laser (or array), separate external detector and gas cell. We consider a 3-inch epi costs \$12,500 (based on a quotation from a commercial vendor), yield is 100%, and at a minimum there are 20 DFBs per die. For complete monolithic, the die size is considered 15mm×5mm with 20DFBs. For hybrid monolithic, we consider that QCL ridge length is ~2mm with ~1mm taper and 20 DFB QCL ridges for a die size ~4mm×5mm.

The same spacing between QCL ridges is considered. For the hybrid case, such as in ref. [18], where several active regions are stacked one on top of the other, the QCL ridge length was 8.5mm, and in the presented beam combining configuration, S-bends were 1.8mm long. The QCL epi requirement is ~16mm×3mm. We assume the same processing cost of the whole wafer ~5K. We also assume that the good epi region is about 75% of the total 3-inch wafer. In the case of hybrid monolithic, we consider that the 4-inch SOI or SOS wafer costs \$500.

#### \*\*The considerations here are as follows:

- 1) If the 3-inch epi is first bonded to the silicon wafer, and the QCL and QCD are fabricated post-bonding, the die size would also increase to 15mm×4mm similar to complete monolithic case, since the length of the coupling tapers, the slotted photonic crystal waveguide and polarization rotator would remain unchanged. †The individual die manufacturing cost would then increase to \$400, similar to complete monolithic device.
- 2) Except situation 1 above, the only alternative is to first dice the 20DFBs and then bond them to the silicon (or other Group IV or III-V).
  - a. If only QCL is bonded to silicon (or other Group IV or III-V), and an external QCD is used, it is not logical since one could simply use a multi-wavelength epi as in the non-monolithic case in Column 3.
  - b. Hence, the meaningful strategy for hybrid monolithic appears to be to first bond the laser (which can be a <u>non-aligned</u> bonding), then fabricate the silicon waveguide, and then do an <u>aligned</u> second bonding of the detector. Hence, two (2) wafer bonding steps would be required.
- 3) Surface treatment or planarization with chemical mechanical polishing (as needed) has not been considered in the cost. Wafer bonding is an extremely low yield process. We previously sent wafers and dies to a commercial wafer bonding tool manufacturer. Only 1 out of 8 bonds succeeded between full 2-inch InP wafers to 4-inch SoS substrates. (12.5% yield). The low yield of bonding processing adds an additional uncertainty to consideration 1 above as well which would make it costlier than Omega's approach.
- 4) We have not made any assumptions regarding the type of silicon passive sensor for absorbance sensing. It could be a strip waveguide, or slot waveguide, or photonic crystal waveguide. The cost numbers only come from the epi processing and the bonding processing.

#### ††The considerations here are as follows:

- 1) If only the multi-wavelength laser ridge is considered that covers the  $\Delta\lambda$ ~6-10µm wavelength bandwidth, then the cost of a single such laser ridge with beam combiners as described in ref. [18] would be \$240 (assuming epi costs \$18K). In such situation, one would need an external detector and gas cell.
- 2) If one ignores limitations of analyte overlap integral versus wavelength in a single waveguide, carrying all wavelength λ=6-10μm, then the simplest wideband waveguide is a strip waveguide and the common method to increase length is via the use of spirals. In general, for spirals, the radius of curvature of the outermost spiral is at least 10 times that of the innermost spiral for a meaningful length. With such consideration, one would observe that with a minimum bend radius of 1mm, the outermost spiral with bend radius 10mm would be expected to occupy a circular region 20mm in diameter at λ=6.5μm. By scaling wavelengths based on Maxwell's equations, this diameter would be 30mm at λ=9.5μm. Thus a single die with Δλ~6-10μm can be expected to occupy an area 16mm×30mm.
- 3) Processing cost can be expected to be much more since separate ridges of different heights would need to be processed for each epi stacked active region. Each epi will be extremely costly.
- 4) There is no apparent advantage in beam combining from sensing perspective on-chip, in a complete monolithic device, since shorter wavelengths are significantly more confined to a waveguide, and overlap less with analyte than longer wavelength in the same waveguide. Separate waveguides are needed, each with their own large diameter spiral for enhanced optical path length which would further increase the cost of a single spectrometer covering Δλ~1μm. The alternative is to use external gas cell.

- 5) When comparing a  $\Delta\lambda$ ~1µm wavelength bandwidth, as in columns 2 and 3, the cost is >\$450.
- 6) It may be noted that we have previously done experiments comparing slotted photonic crystal waveguide and strip waveguides [8]. While a 800µm long slotted photonic crystal waveguide is able to detect 10ppm (parts per million) triethylphosphate (TEP) experimentally, a 8mm long strip waveguide was unable to detect even 28pph (parts per hundred) TEP. The analyte overlap integrals are thus much better in slotted photonic crystal waveguides [8].

# 4. DEVICE DESCRIPTION AND RESULTS

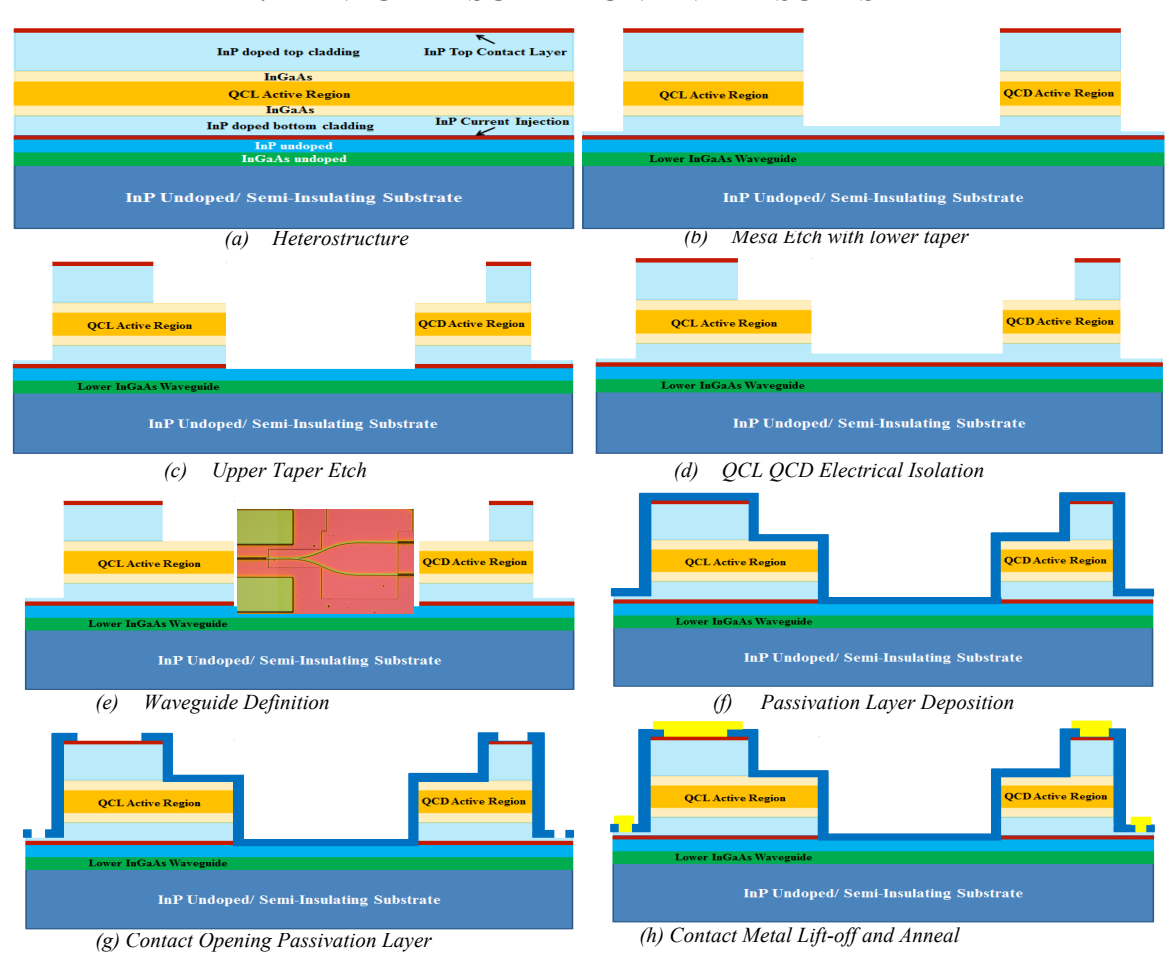


Figure. 3: Primary epitaxial layers of heterostructure. Individual layer thicknesses are different for different  $\Delta \lambda \sim 1 \mu m$  bandwidth in  $\lambda = 3-15 \mu m$  wavelength range. (b) –(h) Fabrication steps of integrated QCL-QCD-waveguide architecture.

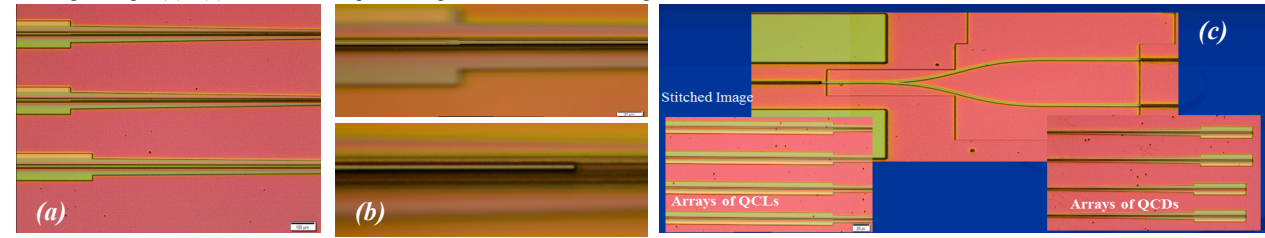


Fig. 4: (a) Microscope images of the device showing integrated QCL/QCD array and strip waveguides.

Fig. 3 shows the fabrication steps of the integrated device. Fig. 3(a) shows the general monolithic epitaxial heterostructure comprising an active core region sandwiched between two high index InGaAs cladding layers, with top and bottom cladding layers and top and bottom current injection/ contact layers. Below the bottom current injection layer

is the undoped passive InGaAs waveguide layer on top of InP substrate with a top cladding InP. For each wavelength range comprising an active core region sandwiched between two high index InGaAs cladding layers, with top and bottom cladding layers and top and bottom current injection/contact layers. Below the bottom current injection layer is the undoped passive InGaAs waveguide layer on top of InP substrate with top cladding InP. Fabrication steps are shown in Fig. 3(b)-(h) which comprises standard processing steps namely (b) QCL and QCD ridge definition, (c) upper taper formation (d) electrical isolation between QCL and QCD (e) passive underlying InGaAs strip waveguide definition (f) passivation layer deposition (g) contact opening definition through passivation layer and finally (h) contact metal lift-off (Ge/Au/Ti/Au 300/500/300/3000Å). Microscope images of different device sections are shown in Fig. 4. Fig. 5 shows the QCD response as a function of QCL bias current in a representative QCL-QCD-waveguide device.

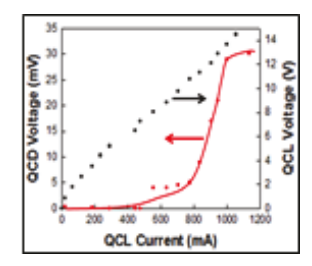


Figure 5: Measured response from QCD coupled to the QCL-coupled waveguides.

Figs. 6(a) and (b) shows top view and cross-section view SEMs of a suspended membrane subwavelength waveguide in InGaAs-InP fabricated separately. Figs. 3(c) and (d) show the top view and cross-section view of a suspended membrane slotted PCW.

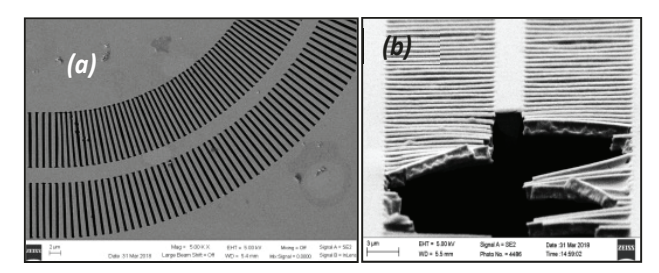


Figure 6: (a) Top view and (b) cross-section view SEM of suspended membrane subwavelength waveguide

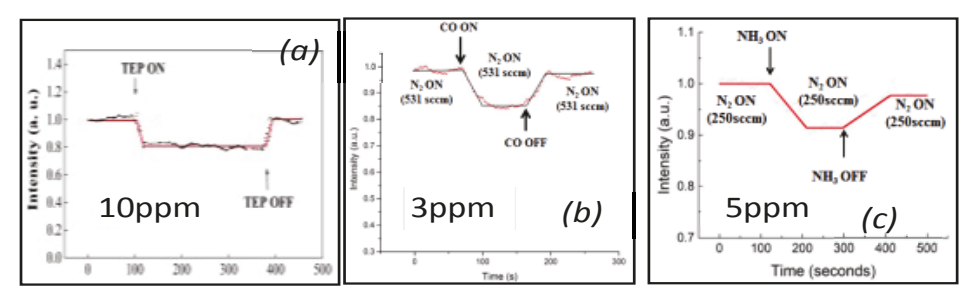


Figure 7: Experimentally detected gas concentrations for (a) TEP (b) CO and (c) NH3 in mid-IR nanophotonic waveguides.

Fig. 7 shows typical gas sensing results obtained separately in previous work with nanophotonic waveguides in mid-IR in various material systems.

# 5. SUMMARY

In summary, we experimentally demonstrated monolithic integration of quantum cascade laser and detector and subwavelength waveguides on a single epitaxial heterostructure on a common substrate for on-chip absorption sensing. Designs can cover 3-15 micron wavelengths without wafer bonding. Comparisons are provided of our common substrate complete monolithic architecture with two other integration platforms: first, heterogeneous integration with external laser and detector integrated with passive sensors and second, the hybrid substrate material integration via bonding.

#### **ACKNOWLEDGEMENTS**

The research was funded by the Army (ARO) STTR Contract #W911NF-17-P-0056. The authors also acknowledge the use of Texas Nanofabrication Facilities supported by the NSF NNCI Award #1542159.

#### REFERENCES

- [1] M.J. Thorpe, K.D. Moll, R.J. Jones, B. Safdi, J.Ye, "Broadband Cavity ringdown spectroscopy for sensitive and rapid molecular detection," Science 311, 1595 (2006)
- [2] M. Lackner, "Tunable diode laser absorption spectroscopy (TDLAS) in the process industries A review," Rev. Chem. Engg. 23(2), 65 (2007).
- [3] URL: <a href="http://www.mksinst.com/product/">http://www.mksinst.com/product/</a>.
- [4] W-C. Lai, S. Chakravarty, X. Wang, C. Lin, R.T. Chen, "On-Chip methane sensing by near-IR absorption signatures in a photonic crystal slot waveguide", Optics Lett. 36, 984 (2011).
- [5] W-C. Lai, S. Chakravarty, R.T. Chen et al., "Photonic Crystal Slot Waveguide Absorption Spectrometer for On-Chip Near-Infrared Spectroscopy of Xylene in Water", Appl. Phys. Lett. 98, 023304 (2011).
- [6] N.A. Mortensen, S.S. Xiao, "Slow-light enhancement of Beer-Lambert-Bouguer absorption," Appl. Phys. Lett. 90 (14), 141108 (2007).
- [7] A. Rostamian, J. Guo, S. Chakravarty, C-J. Chung, D. Nguyen, R.T. Chen, "Parts-Per-Billion Carbon Monoxide Sensing in Silicon-on-Sapphire Mid-Infrared Photonic Crystal Waveguides", CLEO ATh10.4 (2018).
- [8] Y. Zou, S. Chakravarty, P. Wray, R. T. Chen, "Mid-Infrared holey and slotted photonic crystal waveguides in silicon-on-sapphire for chemical warfare simulant detection," Sensors and Actuators B 221, 1094 (2015).
- [9] D. Ristanic, B. Schwarza, P. Reininger, H. Detz, T. Zederbauer, A. Maxwell Andrews, W. Schrenk, G. Strasser, "Monolithically integrated mid-infrared sensor using narrow mode operation and temperature feedback," Appl. Phys. Lett. 106, 041101 (2015).
- [10] L.B. Kreuzer, "Ultralow Gas Concentration Infrared Absorption Spectroscopy", J. Appl. Phys. 42(7), 2934 (1971).
- [11] F.W. Lytle, R. B. Greegor, G. H. Via, J. M. Brown, G. Meitzner, "Gas Phase X-Ray Absorption Spectroscopy with an electron yield detector", J. De Physique 47 (C8), 149 (1986).
- [12] F. Moya, S. A. Druet, J. P. E. Taran, "Gas spectroscopy and temperature measurement by coherent Raman anti-Stokes scattering", Opt. Comm. 13(2), 169 (1975)
- [13] J.S. Namkung, M. Hoke, R. S. Rogowski, S. Albin "FT-IR Optical Fiber Remote Detection of Aluminum Hydroxide by Evanescent Wave Absorption Spectroscopy", Appl. Spectros. 49 (9), 1305 (1995).
- [14] X. Yu, Y. Zhang, Y. C. Kwok, P. Shum "Highly sensitive photonic crystal fiber based absorption spectroscopy", Sens. and Actuators B- Chemical 145(1), 110 (2010).
- [15] A. Kosterov, R. F. Curl, F. K. Tittel, R. Köhler, C. Gmachl, F. Capasso, D. L. Sivco, A. Y. Cho, "Transportable automated ammonia sensor based on a pulsed thermoelectrically cooled quantum-cascade distributed feedback laser", Appl. Optics 41(3), 573 (2001)
- [16] A. Hugi, R. Terazzi, Y. Bonetti, A. Wittmann, M. Fischer, M. Beck, J. Faist, E. Gini, "External cavity quantum cascade laser tunable from 7.6 to 11.4µm", Appl. Phys. Lett. 95, 061103 (2009)
- [17] Y. Ma, G. Yu, J. Zhang, X. Yu, R. Sun, and F.K. Tittel, "Quartz enhanced photoacoustic spectroscopy based trace gas sensors using different quartz tuning forks," Sensors **15**, 7596 (2015); http://www.gasera.fi/technology/photoacoustics/solid-phase-pas/
- [18] W. Zhou, N. Bandyopadhyay, D. Wu, R. McClintock, Manijeh Razeghi, "Monolithically, widely tunable quantum cascade lasers based on a heterogeneous active region design", Scientific Reports 6:25213, 1 (2016)